# The Nature and Strategy of Minimizing the Total Travel Time for Long-Distance Driving of an EV

Junzhe Shi<sup>1</sup>, Teng Zeng<sup>2</sup>, Scott Moura<sup>3\*</sup>

- 1. University of California, Berkeley, Department of Civil and Environmental Engineering, 760 Davis Hall, Berkeley, CA 94720, USA. Berkeley, CA 94720, USA. junzhe@berkeley.edu
- 2. University of California, Berkeley, Department of Civil and Environmental Engineering, 760 Davis Hall, Berkeley, CA 94720, USA. Berkeley, CA 94720, USA. hustlejanton@berkeley.edu
- 3. University of California, Berkeley, Department of Civil and Environmental Engineering, 760 Davis Hall, Berkeley, CA 94720, USA. Berkeley, CA 94720, USA. smoura@berkeley.edu
- \* Corresponding author: Scott Moura, University of California, Berkeley, Department of Civil and Environmental Engineering, 760 Davis Hall, Berkeley, CA 94720, USA, Email: smoura@berkeley.edu

Abstract—The famous Cannonball Run, a cross-country driving challenge from New York City to Los Angeles, highlights the unique challenges of long-distance electric vehicle (EV) route planning. The time record for an internal combustion vehicle is 25 hours, 39 minutes. Compare this to the EV record of 42 hours, 17 minutes, achieved with a Tesla Model S, which elucidates the complexities inherent to optimal EV route planning. To bridge this divide, our study introduces a system designed for real-time vehicle-to-cloud (V2C) interaction aimed at enhancing online long-distance EV route planning. Our approach integrates four pivotal components: (i) a real-time route data processing module, (ii) an energy consumption module that works for different road conditions, (iii) an EV charge time prediction module grounded on real EV charging data, and (iv) a comprehensive optimization module using a Mixed-Integer Linear Programming (MILP). In applying this system to the Cannonball Challenge, our simulation results surpass the realworld EV time record. Importantly, our integrated system's potential extends beyond this challenge, offering robust solutions for personal and commercial EV long-distance drives.

**Keywords:** Electric vehicles, Optimized Routing, Charging stations, Charging time, V2X

#### NOMENCI ATURE

	NOMENCLATURE	
A. Indice	s Index of the pass-through point along the	$b_{hw}$
·	route and the corresponding charging station of each point with the shortest detour distance.	$c_{hw}$
$B.$ Routin $D_{detour}(i)$	ng Data Processing Module  Detour distance to access a charging station	$d_{hw}$
$D_{P2C}(i)$	between point $i$ and the next point $i + 1$ . Distance from point $i$ to a charging station.	$a_{ub}$
$D_{C2NP}(i)$	Distance from a charging station to the next point $i + 1$ .	$b_{ub}$
$D_{P2NP}(i) \ V_{detour}$	Distance from point $i$ and the next point $i + 1$ . Detour speed.	$c_{ub}$
$t_{detour}(i)$	Detour time to access the charging station between point $i$ and the next point $i + 1$ .	$d_{ub}$
$P_{detour} \ E_{detour}(i)$	Average detour consumption power. Energy consumption for detouring to the charging station between point $i$ and the next point $i + 1$ . Numbers of the routing path partition segment.	$D.$ Nonline $SOC(k)$ $C_P$ $\Delta t$ $f_P(SOC(k))$
	segment.	

D(i)	Distance of the route segment from point $i$ to $i + 1$ .	
R(i)	Road type from point $i$ to $i + 1$ .	
$t_{traffic}(i)$	Predicted traffic durations from point $i$ to $i + j$	
ctraffic(c)	1.	
C. Energ	y Consumption Module	
$P_t$	Road traction power.	
$P_d$	Power demand.	
m	Vehicle mass.	
$A_f$	Front area.	
$f_r$	Rolling resistance coefficient.	
$C_D$	Air drag coefficient.	
$\eta_T^{\scriptscriptstyle D}$	Transmission efficiency.	
$\eta_{md}$	Electrical machine efficiency.	
$\eta_r$	Efficiency of regenerative braking.	
V	Vehicle speed.	
α	Road slope.	
ρ	Air density.	
g	Gravitational acceleration.	
$P_{hw}$	Average power consumption for highway	
1644	driving.	
$P_{nh}$	Average power consumption for urban	
ub	driving.	
$a_{hw}$	Fitting parameter used in the highway average	
	power consumption calculation.	
$b_{hw}$	Fitting parameter used in the highway average	
	power consumption calculation.	
$c_{hw}$	Fitting parameter used in the highway average	
	power consumption calculation.	
$d_{hw}$	Fitting parameter used in the highway average	
	power consumption calculation.	
$a_{ub}$	Fitting parameter used in the urban average	
	power consumption calculation.	
$b_{ub}$	Fitting parameter used in the urban average	
	power consumption calculation.	
$c_{ub}$	Fitting parameter used in the urban average	
	power consumption calculation.	
$d_{ub}$	Fitting parameter used in the urban average	
	power consumption calculation.	
	near Charging Module	
SOC(k)	Battery SOC at the time $k$ .	
$C_P$	Battery nominal capacity.	
$\Delta t$	Sampling duration.	
$f_P(SOC(k))$	Nonlinear relationship between charging	
	power vs. SOC curve.	

$f_{\mathcal{C}}(SOC(k))$	Cumulative charging time as the vehicle
, ( ) ,	charges from 5% to $SOC(k)$ .
$t_C$	Charging duration.
$SOC_{arrive}$	Initial SOC of an EV when it has just arrived
unive	at the charging station.
$SOC_{leave}$	Final SOC of an EV when it leaves the
teuve	charging station.
E. Optim	ization Module
I	Total travel time for long-distance EV driving.
$t_{driving}(i)$	Time to travel from point <i>i</i> to the next point
ar titing ( )	i+1.
$t_{charging}(i)$	Charging duration at charging station <i>i</i> while
charging ( )	charging is required.
V(i)	Vehicle's average speed from point $i$ to $i + 1$ .
$t_{charging}(i)$	Charging duration at the charging station <i>i</i>
$SOC_{leave}(i)$	SOC of an EV when it just arrived at the
leuve (-)	charging station $i$ .
$SOC_{leave}(i)$	SOC of an EV when it leaves the charging
- · · · · · · · · · · · · · · · · · · ·	station i.
$t_{overhead}(i)$	Overhead time required for charging at the
over neuu ()	charging station i.
$Time_{extra}$	Constant parameter approximating the extra
cxtr a	duration demanded by charging activities,
	aside from the detour time.
C(i)	Binary variable indicating whether the EV is
	sent to charge at the charging station $i$ .
$SOC_{start}$	SOC of an EV when it is at the starting
	location.
$SOC_{final}$	Minimal SOC required for the EV to reach its
,	destination.
$SOC_{stage\ min}$	Lower bound of the SOC for the EV except
	the start and final locations.
$SOC_{stage\ max}$	Upper bound of the SOC expect the start and
	final locations.
$E_{com}(i)$	Energy consumption from point $i$ to $i + 1$ .
$V_{hw\ max}$	Maximal speed of an EV on highway.
$V_{ub\ max}$	Maximal speed of an EV in urban areas.
$Cp_{initial}$	EV's initial capacity.
$SOH_{now}$	Current SOH of the EV.
$C_{bat}$	Current battery capacity of the EV.
$E_{pre}$	Energy consumption due to preconditioning.
$E_{overhead}(i)$	Energy consumed due to detouring for
	charging and the process of battery
	preconditioning from point $i$ to $i + 1$ .
$V_{grid}$	Grid that represents the discretized velocity
	range of the EV.
$n_V$	Length of this velocity grid.
$v_i$	Binary array that represents the selection of
202	velocities from point $i$ to $i + 1$ .
$SOC_{grid}$	Grid that represents the discretized SOC range
	of the EV.
$n_{soc}$	Dimension of the SOC grid vector.
$S_{leave,i}$	Binary array that represents the SOC when the
S	EV just leaves at the charging station <i>i</i> .
$S_{arrive,i}$	Binary array that represents the SOC when the
+	EV just arrived at the charging station <i>i</i> .
$t_{charging\ grid}$	Grid that represents the discretized function of

#### I. INTRODUCTION

In this section, we start by setting the stage with the context of our problem. We introduce and highlight the challenges to

charges from 5% to a target SOC.

the cumulative charging time as the vehicle

the problem and review the state-of-art approach. Finally, we conclude with the contributions of this work.

## A. Background and Motivation:

The Paris Climate Accord has delineated a critical target: to limit long-term global warming to below 1.5 degrees Celsius. Achieving this benchmark necessitates a drastic 50% reduction in carbon dioxide and other greenhouse gas emissions by 2030 [1]. One pivotal avenue to realizing this ambition is through the electrification of the transportation sector, which currently shoulders over 16% of global emissions [2]. Thanks to proactive governmental policies globally, there has been a discernible surge in the adoption of electric vehicles (EVs) [3], progressively challenging the dominance of traditional internal combustion engine vehicles [4] [5]. Because electric motors convert a high percentage of electrical energy from the grid into power to drive the wheels [6], EVs are more energy-efficient than traditional gasoline or diesel cars and produce fewer greenhouse gases and pollutants [7]. However, the Cannonball Run, a popularized and unsanctioned cross-country trek from New York City to Los Angeles, serves as a vivid illustration of the challenges facing long-distance travel with EVs. While a gasolinepowered vehicle set the record of 25 hours and 39 minutes [8], EVs, despite their rapid technological maturation, have longer journey durations. The current EV record stands at 42 hours and 17 minutes [9]. This stark contrast underscores an important query: how can we harness and optimize EVs for long-distance travel to enable time efficiency?

The quest to minimize travel time is of paramount consequence for both individual travelers and commercial entities. For individuals, shorter trips translate to efficient use of time and alleviate the 'range anxiety' often associated with longer EV journeys [10]. For commercial operations, like long-haul logistics, minimizing travel time is crucial as time directly equates to operational costs and service quality. Delays in deliveries can result in a ripple effects across supply chains, disrupting operations, incurring costs, and potentially damaging reputations [11]. Hence, an efficient EV routing strategy can be a game-changer for both sectors, ensuring not only timely travel but also optimized fleet utilization and reduced operational costs.

However, minimizing the total travel time for EVs on long-distance trips presents a complex challenge arising from the inherent characteristics of electric vehicles. These challenges include limited battery range, longer charging times compared to gasoline vehicles, and the necessity for longer detours to access charging stations, which are less ubiquitous than traditional fuel stations [12]. Despite significant investments like the Bipartisan Infrastructure Deal [13] and the National Electric Vehicle Infrastructure (NEVI) Formula Program [14] aiming to enhance the charging infrastructure, comprehensive solutions to these challenges are still lacking. For instance, while increasing speed can linearly reduce travel time, it also results in a cubic increase in power consumption. This imbalance could lead to quicker battery depletion, necessitating detours for recharging and

subsequently extending the total travel time. Identifying the optimal driving speed that achieves a balance between energy efficiency and time efficiency is therefore critical. Additionally, the process of determining which charging stations to use is not straightforward. The choice of a charging point should consider not only the detour distance but also the current SOC of the EV to ensure sufficient energy levels, avoid unnecessary charging, and minimize detour time for accessing charging stations. Furthermore, the nonlinear characteristics of the charging curve suggest that charging to a high SOC, such as 100%, may not always be the most time-efficient strategy. Determining the optimal amount of charge to be added at each stop to ensure the fastest charging speed is a key component of efficient route planning.

Given this context, this study is dedicated to exploring the nature and strategy of minimizing the total travel time for long-distance EV driving by addressing the following pivotal questions:

- 1. How fast should we drive?
- 2. When should we charge our EV, and at which charging points?
- 3. To what SOC level should we charge our EVs at these points?

#### B. Literature Review:

Early endeavors in EV routing relied on foundational models and predominantly focused on specific application scenarios. These initial efforts were epitomized by the Electric Vehicle Routing Problem (E-VRP) and its various iterations [15]. Many such studies examined the dispatching of an EV fleet for goods transportation. One notable variant is the E-VRP with a time windows, where each customer node has a fixed delivery time window. This introduces sets of upper and lower bound constraints to the problem [16] [17] [18]. Other versions of E-VRP consider charging at depots, customer locations, or dedicated charging stations [19] [20] [21]. Given the constraints set by the aforementioned time windows, dispatch operators need to exhibit increased intelligence in vehicle scheduling. This not only caters to delivery needs but also includes refueling plans at specific locations and times. However, these foundational methods simply adapt previous research paradigms and neglect essential real-world dynamic elements such as real-time traffic conditions, the intricate relationship between speed and energy consumption, and the nonlinear charging dynamics specific to EVs. For the following three paragraphs, a more detailed discussion regarding these three aspects is included, shedding light on the intricacies and advancements in each area.

With the rise of real-time data, transportation paradigms underwent a transformation, reshaping route planning dynamics and significantly enhancing decision-making, addressing some limitations of earlier methods [22]. For instance, [23] estimated traffic speed using crowd sensing techniques, leveraging signal towers and smart devices within vehicles. In [24], the authors harvested traffic incident

data through the Bing Maps REST service, merging historical trajectory data with real-time traffic incident information to predict traffic flow and sidestep obstructed routes. Yet, despite these advancements, the unique challenges inherent to EV routing largely remained unaddressed. In this case, Vehicle-to-Everything (V2X) communication technology is a promising potential solution [25]. With real-time updates and predictions regarding road conditions, traffic duration, and even charging station availability, vehicles can adapt instantaneously, optimizing their operations in alignment with real-world scenarios [26]. However, no literature presents an easy and efficient way to integrate V2X into EV long-distance driving route planning.

The advancement in leveraging real-time data naturally leads to a reevaluation of energy consumption models. Various energy consumption models are fundamental to modern EV routing strategies. While simplistic constant consumption models [27] are favored for their straightforwardness, they frequently fall short in mirroring real-world dynamics. In pursuit of a more realistic portrayal of EV energy consumption rates, many studies have incorporated distinct drive or speed cycles, deriving energy consumption from the vehicle's longitudinal dynamic model. For instance, [28] employed the New European Driving Cycle, simulating both city and suburban driving conditions, and determined energy consumption by considering kinetic energy and motor resistance. In contrast, [29] moved away from fixed drive cycles, opting instead for link-based speeds. Basso, et al. [30] offered a meticulous link and mass-based energy consumption rate model grounded in acceleration, deceleration, and speed metrics. However, such intricate models come with their complexities, making them challenging for applications like long-distance travel. The need for an accurate EV energy/power consumption model is indisputable. However, the model must be straightforward or amenable to reformulation for its practical use in EV route planning. Thus, it is necessary to address this challenge by crafting a model that adeptly merges these dimensions.

As EV adoption has proliferated, the nuances associated with charging have become evident [31]. Notably, the charging rate of EVs is not uniform. It is crucial to accurately predict battery charging time by considering the battery's nonlinear charging profile [32]. In the existing literature, most works assume a constant charging rate for computational benefits, including all aforementioned studies. Integrating the nonlinear nature of battery charging into EV operational optimization presents a formidable challenge. This integration necessitates meticulously crafted model formulations to guarantee both computational efficiency and optimality [33]. For the development of realistic EV routing systems, several studies have delved into the nonlinear power curve. For instance, [34] incorporated a constant current constant voltage (CCCV) curve and proportionally reduced the current when the state of charge (SOC) surpassed 80%, aiming to curtail the total power consumption. Nonetheless, the simple CCCV charging profile is no longer typical in the EV industry for fast charging scenarios. Hecht, et al. [35]

introduced a route planning system, which utilizes recently reported experimental data on EV fast charging curves. However, this work does not offer an effective strategy to embed the EV nonlinear charging profile into optimization with low computational cost. Consequently, there remains a discernible gap in the literature when it comes to accurately modeling and incorporating contemporary EV nonlinear charging profiles into route planning strategies.

Current research predominantly addresses short-distance EV routing, where the battery range is often adequate for the journey with minimal mid-trip charging, focusing primarily on route planning and energy efficiency [36] [37]. In contrast, long-distance EV driving requires more charging stops and demands meticulous management to avoid unexpected vehicle shutdowns and ensure time efficiency [38]. Thus, it is important to consider more factors such as charging locations, charging profiles, battery SOC, and sophisticated vehicle energy consumption models. While the long-distance EV driving planning problem involves more variables and constraints, it is computationally more complex and requires a more efficient optimization method for real-time applications.

In summary, existing studies in EV route planning primarily focus on short-distance travel, often neglecting the unique challenges of long-distance journeys. There is a notable lack of comprehensive systems that integrate real-time data, such as V2X connectivity, with advanced energy consumption models and EV nonlinear charging behaviors. Furthermore, most current methods do not adequately balance the intricate realities of EV behavior with the need for low computational cost in real-time applications. Our study aims to address these gaps by understanding their nature and developing an integrated, efficient, and practical strategy for long-distance EV driving planning.

# C. Contributions

Our research uniquely addresses the challenge of minimizing total travel time for long-distance EV driving, a topic not comprehensively explored in existing literature. We bridge this gap by discussing the nature of long-distance EV driving and developing an integrated framework focused on optimizing travel time. Our pivotal contributions include:

- Development of an integrated and comprehensive system for EV long-distance routing and recharging: We present a system that integrates real-time V2C interactions with route data processing, energy consumption modeling, and charging time prediction.
- Development of a charging time prediction model: Our research introduces a new model for predicting charging time, taking into consideration the nonlinear charging profile of electric vehicles. This model is adaptable enough to accommodate various nonlinear charging profiles.
- 3. Formulation of the travel time minimization problem in a Mixed-Integer Linear Programming (MILP) format: We formulate the problem of minimizing total travel

time into a MILP framework. This approach ensures low computational cost, making it suitable for real-time applications in long-distance EV driving planning.

## D. Organization of the paper:

The remainder of this paper is organized as follows. Section II discusses the methodologies for the problem. Section III analyzes the simulation results of the proposed system. Section IV summarizes the key conclusions of this study.

#### II. METHODOLOGY

In this section, an overview of the system is initially presented to elucidate the functionality of each component within the proposed framework. Subsequently, the methodologies employed within each component are explored in detail in the ensuing subsections.

# A. System overview

In pursuit of optimizing long-distance EV driving planning, this study amalgamates four different modules. Fig. 1 presents a summarized schematic representation of the proposed system's architecture and flow. As shown in Fig. 1, the proposed system takes vehicle type, approximate weight, current time and location, required stops, and batteries' SOC and SOH as inputs. These four modules run in the cloud, and they are (i) a real-time route data processing module, (ii) an EV energy consumption module that works for different road conditions, (iii) an EV charge time prediction module grounded on real EV charging data, and (iv) an optimization module.

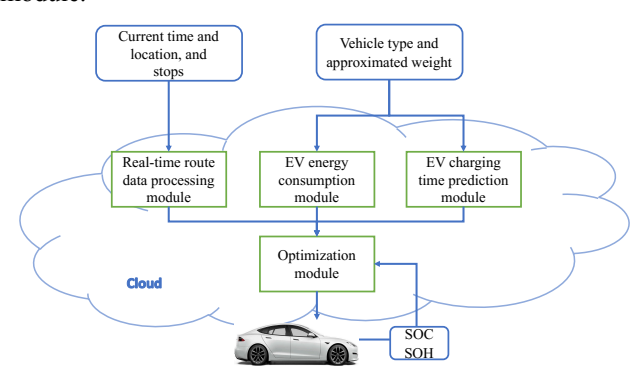


Fig. 1. Frame and flow chart of the proposed system.

Real-time Route Data Processing Module: The process initiates with the acquisition of real-time road data from the Google Maps API [39], using the current time and location, along with specified stops/destinations, to yield a rudimentary routing path characterized by longitude and latitude data. This initial path undergoes refinement via data processing, segmenting it into distinct portions. This segmentation aids in formulating a matrix that encapsulates the distance, charging station detailer time and energy consumption, road type, and ongoing traffic conditions of each segment. This matrix becomes the foundation for the EV long-

distance driving optimization, with further intricacies of the module discussed in Section II.B.

- 2. Energy Consumption Module: This module refines the energy model by accounting for the vehicle's specific characteristics and the type of road it traverses. It quantifies the interplay between driving speed and energy expenditure under various conditions. Acting as the cornerstone of the optimization module, it computes the vehicle's optimal speed for each road segment, informed by inputs such as vehicle type and estimated weight. An in-depth exposition of the module's development is provided in Section II.C.
- 3. Charge Time Prediction Module: In parallel, addressing the intricate nature of EV nonlinear charging behavior, a charging time prediction model is also formulated. This model draws from a real EV charging dataset for accuracy. The main function of the module is to accurately predict the charging duration with a given starting and ending SOC of charging with a given nonlinear charging profile. The details of this module are further discussed in Section II.D.
- 4. Optimization Module: By utilizing the linearization methods, we convert the original nonlinear optimization problem into the MILP framework, which is essential for achieving real-time optimization capabilities. Ultimately, leveraging the insights from the EV energy consumption model, the charging time prediction model, as well as real-time parameters like the current SOC and state of health (SOH) of the EV, the MILP optimization strategy determines the ideal charging strategy and speed schedules to minimize the overall travel time. The details of the optimization approach are further elucidated in Section II.E.

According to the design of our proposed system, initiation can occur in real-time by human operators or higher tier dispatching systems. The routing and data process module, informed by real-time traffic data, determines the optimal route and potential charging station selection. This, coupled with the energy consumption and charging time prediction modules, enables our optimization module to formulate the best strategy based on current conditions. Utilizing the concept of Model Predictive Control (MPC) [40], the system conducts reruns at short intervals, such as every 5 minutes, considering the entire trip as the predictive horizon to bolster robustness. During each rerun, the system incorporates the latest traffic conditions and vehicle states to manage uncertainties and external disturbances, like unexpected traffic changes. The system is also designed to recalibrate and initiate a rerun if deviations from the planned route occur.

B. Routing and Data Process Module:

The routing and data processing module is executed in a series of steps:

- 1. Basic Routing Path Acquisition: Given the current time, location, and predefined stops or destinations, the system retrieves the route polyline via the Google Maps API. A more detailed demonstration of the basic routing path acquisition is presented in Fig. 8 in Section III.B.1).
- 2. Polyline Decoding: The acquired polyline is decoded, yielding specific latitude and longitude coordinates that define the primary routing path.
- 3. Routing Path Partition: The routing path undergoes segmentation to maintain granularity. The Haversine distance between subsequent pass-through points is confined to under 30 miles for enhanced precision. Further details on the selection process of partition interval are provided in Section III.B.3).
- 4. Charging Facility Location Acquisition: The Google Maps API aids the system in scanning the surroundings of each point, pinpointing available charging stations. A more detailed demonstration of the charging facility location acquisition in Fig. 9 in Section III.B.1).
- 5. Identify the Charging Facility with the Shortest Detour Distance: For each designated pass-through point, distances between point i and the next junction point i+1 ( $D_{P2NP}(i)$ ), point i to a charging station ( $D_{P2C}(i)$ ), and from a charging station to the next junction point i+1 ( $D_{C2NP}(i)$ ) are computed using Haversine distances. To save costs associated with Google's API services, the Haversine distance is utilized to reduce frequent API calls. The added detour distance for a charging station, relative to passing through point i, is formulated as:

$$D_{detour}(i) = D_{P2C}(i) + D_{C2NP}(i) - D_{P2NP}(i)$$
 (1)

Subsequently, charging stations with the minimal detour distances for their related pass-through points are cataloged.

- 6. Road and Traffic Information Acquisition: Through the Google Maps API, the system determines exact distances between neighboring pass-through points. Concurrently, it gathers data concerning road types and predicted traffic durations based on expected arrival times.
- 7. Road Type Identification: Each road segment connecting two successive pass-through points undergoes categorization as "highway" or "city road" based on inherent characteristics.
- 8. Detour Distance Acquisition and Calculation: Using the Google Maps API, in tandem with the aforementioned detour distance equation, the detour distances of each potential charging station and junction points are computed as shown in Fig. 2.

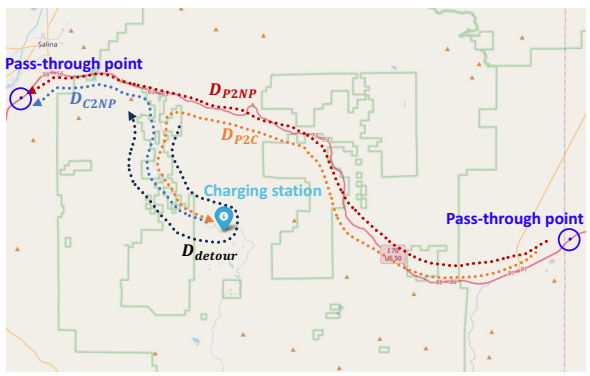


Fig. 2. Detour distance acquisition and calculation.

9. Detour Time and Energy Consumption Calculation: Recognizing that detours invariably lead an EV away from its original path, we postulate the detour speed to be 30 mph to approximate the average local driving speed [41]. From the deduced detour distances  $(D_{detour}(i))$  and speeds  $(V_{detour})$ , we directly estimate the detour time  $(t_{detour}(i))$  for each segment, using the equation,

$$t_{detour}(i) = \frac{D_{detour}(i)}{V_{detour}}$$
 (2)

Furthermore, based on the detour time and speed, the additional energy consumption,  $E_{detour}(i)$ , resulting from detours is computed as,

$$E_{detour}(i) = P_{detour} t_{detour}(i)$$
 (3)

Here,  $P_{detour}$  is the average detour consumption power and calculated based on Eq (7).

In a culmination of these steps, the foundational routing path is divided into N segments, with each approximately covering 30 miles. The outcome is a comprehensive matrix detailing exact distances (D(i)), road types (R(i)), predicted traffic durations  $(t_{traffic}(i))$  between pass-through points, and, where charging is needed, the associated detour time  $(t_{detour}(i))$  and energy consumption  $(E_{detour}(i))$ . This matrix serves as a crucial input for the charging schedule and speed optimization module.

# C. EV Energy Consumption Module:

For optimal speed planning, it is important to have an EV energy consumption model that maps the energy consumption with a given road type and speed.

The study uses a basic EV model as a baseline to calculate the instantaneous power consumption. The formulation of the vehicle power consumption model can be expressed as [42],

$$P_t = m g f_r V \cos(\alpha) + 0.5 C_D A_f \rho V^3$$

$$+ m V \frac{dV}{dt} + m g V \sin(\alpha)$$
(4)

$$P_d = \begin{cases} P_t \, \eta_T \, \eta_{md}, & P_t > 0 \\ \frac{P_t}{\eta_r}, & P_t \le 0 \end{cases} \tag{5}$$

Here, parameters including m (mass),  $A_f$  (front area),  $f_r$  (rolling resistance coefficient),  $C_D$  (air drag coefficient),  $\eta_T$  (transmission efficiency),  $\eta_{md}$  (electrical machine efficiency), and  $\eta_r$  (efficiency of regenerative braking) are derived based on vehicle type and weight. Variables V and  $\alpha$  represent vehicle speed and road slope, respectively, while  $\rho$  and g stand for air density and gravitational acceleration. The variable  $P_t$  signifies the road traction power that opposes road friction, air drag, and gravitational forces. The eventual power demand  $P_d$  of an EV, factoring in transmission efficiency, electrical machine efficiency, and the efficiency of regenerative braking, is computed from  $P_t$ .

Driving conditions can be mapped with specific driving cycle profiles [43]. For instance, the EPA Highway Fuel Economy Test (EHFET) profile typifies highway conditions, while the Urban Dynamometer Driving Schedule (UDDS) reflects urban driving conditions [44]. Adjusting the speed profiles of these cycles enables establishing the relationship between average power consumption and average speeds across diverse road conditions.

Fig. 3 visualizes the adaptation of the original EHFET cycle speed profile to generate multiple speed profiles. Upon determining the average speed for each profile and utilizing the baseline EV model, along with specified vehicle parameters, one can determine the average power demand across varying average speeds for typical highway conditions. For this study, which is focused on long-distance travel, road slope impacts over time are assumed to be negligible and set to zero.

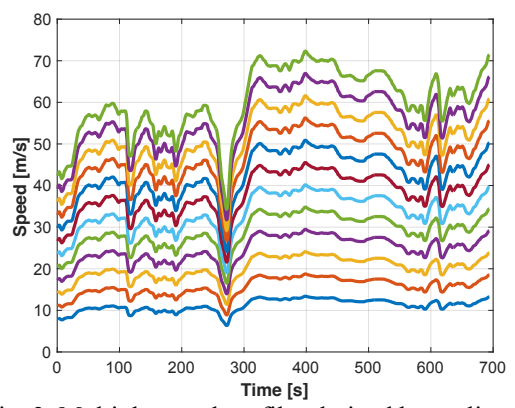


Fig. 3. Multiple speed profiles derived by scaling the EHFET cycle's original speed profile.

Fig. 4, using parameters from the new Tesla Model S as an example, employs a cubic function to trace the relationship between average power consumption and driving speed on highways. The fitted cubic relationship is justified by physics, since power to overcome air drag scales with speed cubed (see Eq. (4)). The same procedure applied to the UDDS cycle produces the consumption model for urban driving. As a

result, we obtain the following two equations to calculate the average power consumption for highway  $(P_{hw})$  and average power consumption for urban driving  $(P_{ub})$ , respectively,

for highways:

$$P_{hw} = a_{hw}V^3 + b_{hw}V^2 + c_{hw}V + d_{hw}$$
 (6)

for urban areas:

$$P_{ub} = a_{ub}V^3 + b_{ub}V^2 + c_{ub}V + d_{ub}$$
 (7)

Here, V is the vehicle average velocity, and  $a_{hw}$ ,  $b_{hw}$ ,  $c_{hw}$ ,  $d_{hw}$ ,  $a_{ub}$ ,  $b_{ub}$ ,  $c_{ub}$  and  $d_{ub}$  are fitting parameters.

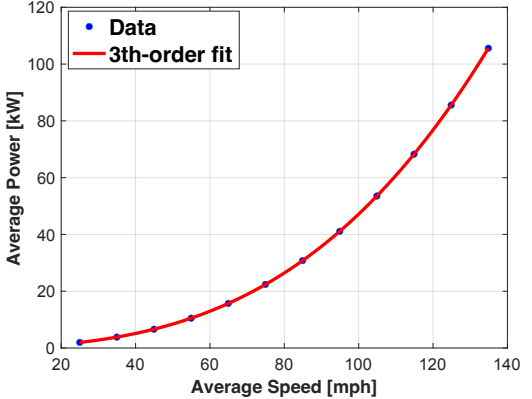


Fig. 4. The average speed vs. average power consumption for a highway driving condition.

This study categorizes driving conditions into highway and urban segments, using the EHFET and UDDS cycles, respectively. However, it is worth noting that employing more specific driving cycle data tailored to varied road types and real-time traffic conditions and classifying them into more categories to build the energy consumption model can further improve the precision of the energy consumption model across diverse conditions.

# D. EV Nonlinear Charging Module:

The EV charging rate is influenced by SOC and temperature [32]. With battery preconditioning, we assume EVs are charged at a consistent and optimal temperature. The focus of this section is to model the charging rate-SOC relationship for accurate charging duration estimation. This subsection describes a method to estimate charging duration based on the initial SOC ( $SOC_{leave}$ ) and the desired end SOC ( $SOC_{arrive}$ ). This method specifically accounts for the nonlinear charging profile inherent to EVs, using the Tesla Model S as an illustrative example.

The nonlinear charging behavior of an EV is captured through a curve relating charging power to SOC [45]. Fig. 5 showcases the real-world nonlinear relationship between charging power vs. SOC curve, denoted as  $f_P$ . This curve was derived from the average charger power of experiments from a 2023 Tesla Model S that was charged from 5% to 90% SOC

using Tesla V3 (i.e. 250 kW maximum power) superchargers. Incorporating the Tesla Model S's nominal capacity,  $C_P$  (in kWh), we can express the vehicle's SOC (in %) as,

$$SOC(k) = SOC(k-1) + 100\% \frac{f_P(SOC(k-1))}{3600 C_P} \Delta t$$
 (8)

Here,  $f_P$  indicates the charging power (in KW) for a specific SOC, while  $\Delta t$  (in seconds) represents the sampling duration.

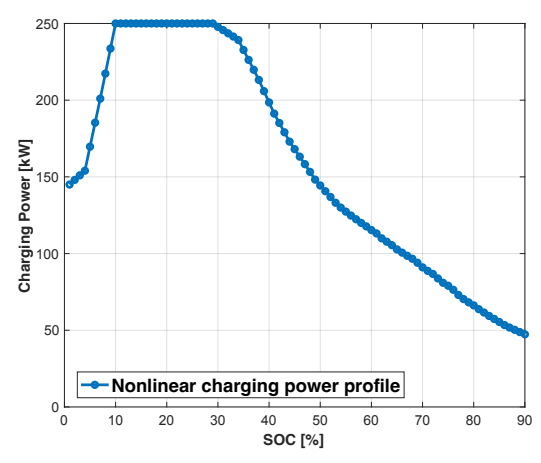


Fig. 5. Charging power vs. SOC.

Based upon the SOC updating model and the nonlinear charging curve, Fig. 6 depicts the curve  $f_C$ , which represents the cumulative charging time as the vehicle charges from 5% to 95% SOC. Notably, the  $f_C$  curve is not universal; it varies across different vehicle types or brands due to the unique charging strategies of individual EV manufacturers. These curves can also change with different charging infrastructure equipment, due to charger cable current and temperature limits [32]. Consequently, it is crucial to establish a library of  $f_C$  curves for various vehicle models and chargers. In application, the system will select the appropriate  $f_C$  curve based on the provided vehicle type or brand and charger.

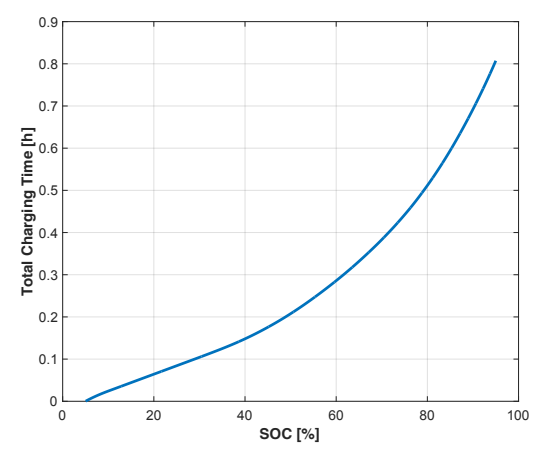


Fig. 6. Cumulative charging time vs. SOC, when starting at 5% SOC.

Given that  $f_C$  inherently captures the relationship between SOC and cumulative charging time, it can inform us about the total charging time required for the battery to attain any given SOC. Utilizing this relationship allows us to determine the duration needed to charge the battery between two SOC values. Therefore, the charging duration,  $t_C$ , for a Tesla Model S transitioning from  $SOC_{arrive}$  to  $SOC_{leave}$  can be computed as,

$$t_C = f_C(SOC_{leave}) - f_C(SOC_{arrive})$$
 (9)

In this equation,  $f_C(SOC_{leave})$  conveys the total time necessary to charge the battery from its starting point (in this context, 5%) to  $SOC_{leave}$ . Similarly,  $f_C(SOC_{arrive})$  signifies the time required to charge from the starting point to  $SOC_{arrive}$ . The difference between these times provides the duration to charge from  $SOC_{arrive}$  to  $SOC_{leave}$ , which is represented by  $t_C$ . To verify the accuracy of our charging time prediction model, we tested it using 57 charging data points obtained from another Tesla vehicle not used for model training. The results of the cross-evaluation showed an average absolute error of only about 2.3 minutes, highlighting the accuracy of the proposed model.

#### E. MILP-based Optimization:

Central to this proposed system is the charging schedule and speed optimization module. In this subsection, we first formulate the control goal as an optimization problem, and detail the cost function, variables, and constraints. Moreover, we showcase the linearization methods employed to convert the original nonlinear optimization problem into the MILP framework, which is essential for achieving real-time optimization capabilities.

The objective (J) is to minimize the total travel time for longdistance EV driving, which is simply the summation of the driving time and the additional time taken by charging. The optimization problem is formulated as the following,

$$J = \sum_{i=1}^{N} t_{driving}(i) + t_{charging}(i) + t_{traffic}(i)$$
 (10)

Here, N signifies the number of road segments, with i denoting the route node index. The variable  $t_{driving}(i)$  is the time to travel from pass-through point i to the next pass-through point i+1, and  $t_{charging}(i)$  is the charging duration at charging station i while charging is required. The driving time of each road segment i is expressed as,

$$t_{driving}(i) = \frac{D(i)}{V(i)} \tag{11}$$

Here, D(i) represents the distance of the route segment from node i to i + 1, and V(i) is the vehicle's average speed on that segment.

The time taken by charging,  $t_{charging}(i)$ , is given by,

$$t_{charging}(i) = f_{C}(SOC_{leave}(i)) - f_{C}(SOC_{arrive}(i)) + t_{overhead}(i)$$
 (12)

where  $SOC_{leave}(i)$  and  $SOC_{arrive}(i)$  represent the SOC of the EV when it arrives and leaves the charging point i. Here, an additional term,  $t_{overhead}(i)$ , is incorporated into Eq. (12) to account for the overhead time required for charging. This time encapsulates both detour time and other related activities, such as the overhead time to park, plug in, initiate a charge session, plug-out, and depart. The representation is given as,

$$t_{overhead}(i) = (t_{detour}(i) + Time_{extra}) \cdot C(i)$$
 (13)

In the equation,  $Time_{extra}$  stands as a constant parameter approximating the extra duration demanded by charging activities, aside from the detour time. Meanwhile, C(i) is a binary variable indicating whether the EV is sent to charge during that specific segment.

For the initial route node indexed 1, both  $SOC_{leave}(1)$  and  $SOC_{arrive}(1)$  equal the vehicle's current SOC,  $SOC_{start}$ . This results in the initial constraints,

$$SOC_{arrive}(1) = SOC_{start}$$
 (14)

$$SOC_{leave}(1) = SOC_{start} \tag{15}$$

For the final point, the SOC should exceed a designed value,  $SOC_{final}$ , to prevent battery over-discharge. Thus, the final constraints are,

$$SOC_{arrive}(N+1) \ge SOC_{final}$$
 (16)

$$SOC_{leave}(N+1) \ge SOC_{final}$$
 (17)

The stage constraints capture the dynamics of the battery's SOC for stages from i = 2 to N.

$$SOC_{stage\ max} \ge SOC_{arrive}(i) \ge SOC_{stage\ min}$$
 (18)

$$SOC_{stage\ max} \ge SOC_{leave}(i) \ge SOC_{stage\ min}$$
 (19)

In these equations,  $SOC_{stage\ max}$  and  $SOC_{stage\ min}$  represent the upper and lower bounds of the SOC, respectively.

According to Eq. (6) and Eq. (7), the energy consumption at each segment,  $E_{com}(i)$ , is determined by multiplying the average driving power with the driving time at each segment as follows,

for highways:  

$$E_{com}(i) =$$

$$(a_{hw}V(i)^3 + b_{hw}V(i)^2 + c_{hw}V(i) + d_{hw})\frac{D(i)}{V(i)}$$
(20)

for urban areas:

$$E_{com}(i) = (a_{ub}V(i)^3 + b_{ub}V(i)^2 + c_{ub}V(i) + d_{ub})\frac{D(i)}{V(i)}$$
(21)

Besides, we also limit the velocity of the EV based on the road type,

for highways: 
$$V(i) \le V_{hw\ max} \tag{22}$$

for urban areas:

$$V(i) \le V_{ub \ max} \tag{23}$$

where  $V_{hw\ max}$  and  $V_{ub\ max}$  are the maximal driving speeds of the EV in highways and urban areas, respectively.

Considering the vehicle's initial capacity ( $Cp_{initial}$ ) and its SOH, the current battery capacity,  $C_{hat}$ , is,

$$C_{bat} = Cp_{initial} \left( \frac{SOH_{now}}{100} + 80\% \right)$$
 (24)

where  $SOH_{now}$  is the current SOH of the EV and is in the range of 0 to 100%, and 0% SOH represents the capacity of the EV's battery drop to 80% of its initial capacity.

With the current energy capacity of the EV, the SOC changes in each segment due to driving can be updated as,

$$SOC_{legne}(i) \ge SOC_{arrive}(i)$$
 (25)

$$SOC_{arrive}(i+1) = SOC_{leave}(i) - 100\% \frac{E_{com}(i) + E_{overhead}(i)}{C_{bat}}$$
(26)

$$E_{overhead}(i) = (E_{detour}(i) + E_{pre}) \cdot C(i)$$
 (27)

In this equation,  $E_{overhead}(i)$  signifies the additional energy consumed due to detouring for charging and the process of battery preconditioning. The energy expenditure arising from the detour is derived using Eq. (3). The term  $E_{pre}$  is a fixed parameter, approximating the energy used during battery preconditioning. The binary variable, C(i), indicates if the EV will undergo charging at a given charging station. Battery preconditioning is essential to both reduce charging duration and to curb potential battery degradation. By maintaining the battery pack temperature at an optimal range prior to charging, these techniques ensure efficient energy intake. Consequently, when an EV is set to charge, there's an extra energy demand due to battery preconditioning.

To account for model uncertainties and avoid battery damage, we restrict the SOC for segments i = 2 to N between 10% and 90%. Additionally, the charging power  $f_p$  is reduced

below 10% and above 90% SOC (see Fig. 4), so allowing a wider SOC range will not help minimize travel time.

The aforementioned equations define the optimization problem in alignment with our control objectives. However, the nonlinearities in Eq (11), Eq (12), Eq (20), and Eq (21) hinders real-time optimization. To address this, the subsequent paragraphs will introduce linearization techniques to transform the problem into a MILP framework, thus enabling real-time optimization capabilities.

To address the nonlinear equations related to speed and energy consumption (Eq (11), Eq (20), and Eq (21)), we transform the continuous variable, V(i), by discretizing it into a finite series of potential velocities for the EV,

$$V_{arid} = [0, 1, \dots, V_{hw max} - 1, V_{hw max}]$$
 (28)

where  $V_{grid}$  is a grid that represents the discretized velocity range of the EV. The length  $(n_V)$  of this velocity grid is represented as,

$$n_V = \left| V_{grid} \right| \tag{29}$$

We introduce a binary array,  $v_i$ , of size  $1 \times n_V$  to represent the selection of velocities from a predefined grid for each road segment i. In this representation,  $v_i$  is a one-hot encoded array, meaning only one element is 'l' and the others are '0'. For all i, we have,

$$\sum_{j=1}^{n_V} v_i(j) = 1 \tag{30}$$

where the '1' at the *j*th position indicates the selection of the *j*th velocity from the velocity grid,  $V_{grid}$ . Each road segment speed, V(i), is then associated with a unique velocity from the grid, converting the following nonlinear equations into linear forms,

$$V(i) = V_{grid} \cdot v_i \tag{31}$$

$$\frac{D(i)}{V(i)} = \frac{D(i)}{V_{grid}} \cdot v_i \tag{32}$$

This transformation facilitates the linearization of Eq (20) and Eq (21) related to energy consumption on different types of roads,

For highway:

$$\begin{split} E_{com}(i) = \\ \left(a_{hw}V_{grid}^3 + b_{hw}V_{grid}^2 + c_{hw}V_{grid} + d_{hw}\right) \frac{D(i)}{V_{grid}} \cdot v_i \end{split} \tag{33}$$

For urban areas:

$$E_{com}(i) =$$

$$(a_{ub}V_{grid}^3 + b_{ub}V_{grid}^2 + c_{ub}V_{grid} + d_{ub}) \frac{D(i)}{V_{grid}} \cdot v_i$$
 (34)

The nonlinearities in Eq (12) concerning SOC are addressed similarly. We discretize the SOC variables, resulting in,

$$SOC_{grid} = \\ [SOC_{min}, SOC_{min} + 1\%, \cdots, SOC_{max} - 1\%, SOC_{max}] \end{(35)}$$

where  $SOC_{grid}$  represents the discretized SOC range of the EV. The dimension of the SOC grid vector is  $n_{soc}$ ,

$$n_{soc} = \left| SOC_{grid} \right| \tag{36}$$

We employ two binary arrays,  $s_{leave,i}$  and  $s_{arrive,i}$ , with a size  $1 \times n_{soc}$  to approximate  $SOC_{leave}(i)$  and  $SOC_{arrive}(i)$ . In the representations,  $s_{leave,i}$  and  $s_{arrive,i}$  are also one-hot encoded arrays. These arrays capture SOC deviations within a 1% interval, ensuring precision while simplifying the equations. For all i, we have,

$$\sum_{i=1}^{n_{soc}} s_{leave,i}(j) = 1 \tag{37}$$

$$\sum_{j=1}^{n_{soc}} s_{arrive,i}(j) = 1$$
 (38)

$$SOC_{arid} \cdot s_{leave i} \le SOC_{leave}(i)$$
 (39)

$$SOC_{grid} \cdot s_{arrive,i} + 1\% \ge SOC_{arrive}(i)$$
 (40)

$$SOC_{grid} \cdot S_{arrive,i} \leq SOC_{grid} \cdot S_{leave,i}$$
 (41)

Subsequently, the function  $f_C$  can be discretized into a grid,  $t_{charging\ grid}$ , with a size  $1\times n_{soc}$ , based on the  $SOC_{grid}$  as depicted in Fig. 7. In essence, for every SOC point within the  $SOC_{grid}$ , there is a one-to-one corresponding point in  $t_{charging\ grid}$ . This represents the time spent to charge from the SOC upon arrival to the departure SOC. Hence, we can establish,

$$f_c(SOC_{leave}(i)) = t_{charging\ grid} \cdot s_{leave,i}$$
 (42)

$$f_c(SOC_{arrive}(i)) = t_{charging\ grid} \cdot s_{arrive,i}$$
 (43)

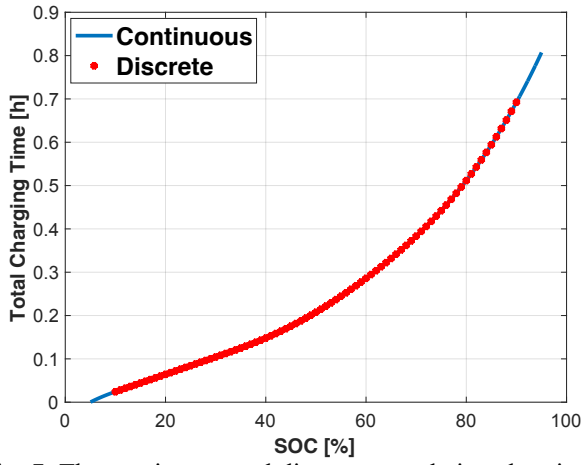


Fig. 7. The continuous and discrete cumulative charging vs. SOC.

In addition, the binary variable, C(i), which indicates whether the EV is set to be charged at the station, can be determinized as follows,

$$C(i) \ge \frac{SOC_{grid} \cdot s_{leave,i} - SOC_{grid} \cdot s_{arrive,i}}{100\%}$$
 (44)

Furthermore, Eq (12) can be linearized and rewritten as,

$$t_{charging}(i) = t_{charging grid} \cdot (s_{leave,i} - s_{arrive,i}) + t_{overhead}(i) \quad (45)$$

With the conversion of all nonlinear equations into their linear counterparts, our optimization problem effectively translates into a classic MILP problem and lets a standard MILP solver be able to solve it efficiently. This adaptation allows for efficient problem-solving and paves the way for real-time optimization capabilities, which are vital for our proposed system's effectiveness. The computational efficiency and the impact of partition intervals on computational time and system performance are thoroughly analyzed in Section III.B.3).

### III. RESULTS AND DISCUSSION

To test our proposed system, we consider the challenging backdrop of the Cannonball Run. This cross-country race serves as our demonstration case, providing a rigorous testbed for our model. In the III.A System Setup subsection, details of the Cannonball Run are presented alongside our model assumptions, vehicle parameters, and other crucial factors. Later, in the III.B Performance subsection, we detail our primary findings, delve into the nuances of nonlinear charging and its influence on routing, and discuss the impact of basic routing path partition intervals on decision-making.

### A. System setup:

Cannonball Run Overview: Originating as a clandestine coast-to-coast car race from New York City to Los Angeles, the Cannonball Run offers an exemplary setting for our

system's validation. Spanning approximately 2,800 miles, the race presents diverse challenges, making it an apt demonstration case. Central to the Cannonball Run ethos is minimizing travel time, prompting racers to disregard legal speed constraints. Maximizing speed is the key strategy for internal combustion engine vehicles. However, the strategy is much more nuanced and interesting for EVs. Increasing speed decreases travel time linearly but increases power consumption cubically. Due to the limited driving range of EVs, this means more necessary charging stops. Meanwhile, the nonlinear charging curve characteristics suggest that charging to a high SOC, such as 90%, may not be time optimal. Finally, planning the route and charging stop locations is a challenge.

**Record-Breaking Run (Benchmark):** In a groundbreaking achievement, Ryan Levenson and Josh Allan piloted a Tesla Model S, setting a new EV Cannonball record with a completion time of 42 hours and 17 minutes. The top speed of the challengers is reported to reach 155 mph [46]. This record will be the benchmark for our proposed system, and it accentuates the intense character of the race and the efficiencies attainable through optimized EV long-distance routing.

**Assumptions and scenario settings:** Our simulation hinges on these specific foundational settings:

- 1. The EV departs with a fully charged battery:  $SOC_{start} = 100\%$ .
- 2. The SOC at the destination must be greater than 5%:  $SOC_{final} = 5\%$
- 3. To avert overcharging or excessive depletion, the SOC boundaries are set at:  $SOC_{stage\ min} = 10\%$  and  $SOC_{stage\ max} = 90\%$ .
- 4. With a Tesla vehicle and its charging network, the extra time spent on parking, setting up chargers, and initiating a charge session is approximately 1 minute: Time<sub>extra</sub> = 1 min.
- 5. The energy required for battery preconditioning is about 1 kWh:  $E_{pre}=1$  kWh. The estimated 1 kWh energy consumption, based on our test data, is used for demonstration purposes only. Considering that preconditioning energy consumption is influenced by ambient temperature [47], integrating predicted temperature data as a parameter for each charging point could offer a more accurate approximation.

- 6. Though we do not condone it in practice, we disregard the legal speed limits in simulation for a fair comparison to the benchmark. The max speeds are set at 130 mph for highways and 70 mph for urban areas:  $V_{hw\ max} = 130$  mph and  $V_{ub\ max} = 70$  mph.
- The departure time is 10 PM in New York City to avoid traffic.
- 8. All the Tesla V3 superchargers can supply a maximum of 250 kW of charging power.
- 9. The traffic data fetched from Google Maps API is presumed to portray actual traffic conditions accurately.
- 10. The model, rooted in Tesla Model S parameters, effectively gauges average energy consumption based on set average speeds and road classifications.

*Vehicle Model and Parameters:* Our simulation adopts the Tesla Model S as the EV archetype. Relevant parameters are elaborated in the following table.

TABLE I.
Parameters of a Tesla Model S [48] [49]

Parameters	Values
Air drag Coefficient (Cd)	0.2
Rolling Resistance Coefficient (f)	2.34 m <sup>2</sup>
Mass (m)	2934 kg
Motor Efficiency (η <sub>M</sub> )	85%
Transmission Efficiency $(\eta_T)$	95%
Regenerative Efficiency $(\eta_R)$	65%
Battery capacity (Cp)	100 kWh
Battery State of Health (SOH)	100%

# B. Performance:

#### 1) Main results:

In the Cannonball Run challenge, vehicles commence their journey from the Red Ball Garage in New York City and culminate at the Portofino Hotel in Redondo Beach, near Los Angeles, without any prescribed intermediary stops. Given a set departure time of 10:00 PM local time, and specified start and end locations, our system uses the Google Maps API to derive an initial routing path, illustrated in Fig. 8. In this representation, the green and red markers denote the starting and ending points respectively, while the blue trajectory marks the planned route.



Fig. 8. The basic routing path from New York City's Red Ball Garage to the Portofino Hotel in Redondo Beach near Los Angeles using Google Map API.

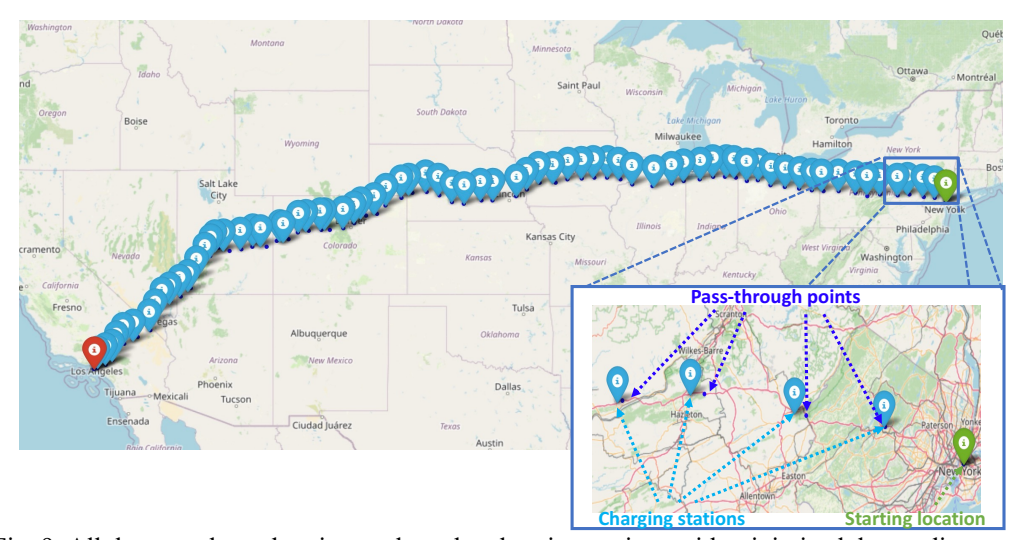


Fig. 9. All the pass-through points and nearby charging stations with minimized detour distances.

To facilitate our optimization, we segmented this route into intervals of approximately 30 miles, resulting in a series of pass-through points, depicted as dark blue dots in Fig. 9. Leveraging the methodology elaborated in Section II.B, we then identified nearby charging stations for each passthrough point, striving for minimal detour distances. These selected charging stations are highlighted using blue markers in Fig. 9. Consequently, the detour distances for the entire trip ranged from a minimum of 0.005 miles to a maximum of 49.5 miles, with an average of 6.9 miles. Furthermore, we extracted essential data such as the actual detour distances required to access each charging station, along with the distance, road types, and estimated travel times between each sequential pair of pass-through points. This data is then employed for optimizing charging schedules and travel speeds.

Upon executing the optimization using the provided data and models, we determined the optimal driving speed for each segment between junction pass-through points. These findings are depicted in Fig. 10. Notably, speeds selected for the initial and ending two segments fall below 70 mph. The rationale behind this is their classification as urban zones based on the available road data, where speed limits are capped at 70 mph. Conversely, for the intervening segments, chosen speeds oscillate between 92.87 mph and 130 mph, which matches the intuition that the optimizer is trying to minimize total trip time. The fluctuation in driving speed is not arbitrary but stems from an energy conservation perspective. Naturally, adopting higher speeds truncates driving durations, yet increases energy consumption. To minimize the total travel time, it is imperative to factor in the time spent on charging. When driving at reduced speeds, the EV consumes less energy, leading to less frequent need for charging and thus curtails the total charging time. This strategy is particularly beneficial when either the detour to a

charging station is excessively lengthy or when the charging rate within a specific SOC range is subdued.

The energy consumption across each segment is depicted in Fig. 11. Notably, energy consumption does not consistently correlate with the driving speed of a segment. This observed variance is attributed to the figure reflecting total energy consumption, which encompasses energy expended due to battery preconditioning and detours made for charging. As such, segments requiring charging inherently register elevated energy consumption. On average, the segments manifest an energy consumption of approximately 25.56 kWh. Using the Tesla Model S as a benchmark, with its 100 kWh battery capacity, this data suggests that the EV would expend around 25.56% of its battery capacity to traverse a 30-mile segment under the optimized strategy. Note that the energy efficiency is seemingly low (853 Wh/mile), particularly due to the vehicle's ultra-high speed along segments. The efficiency will obviously improve when realworld speed limits are applied.

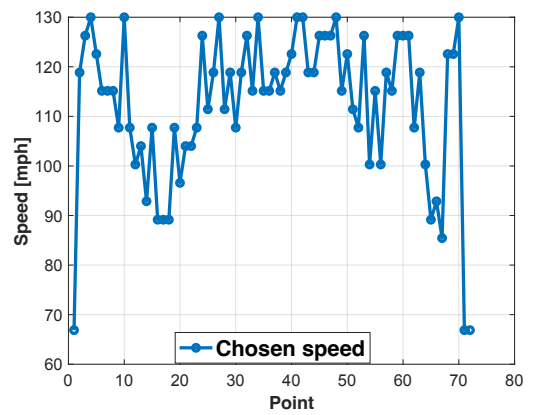


Fig. 10. Chosen speed for the point-to-point segments.

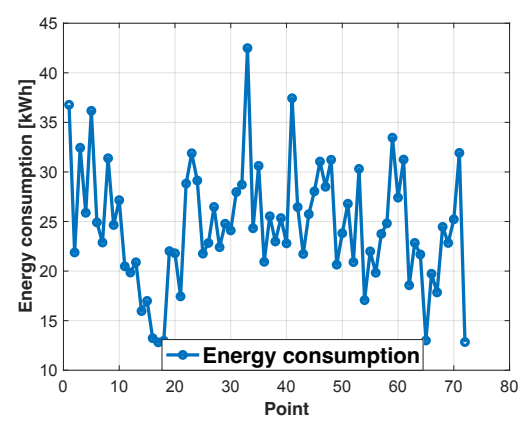


Fig. 11. Total energy consumption for the point-to-point segments with roughly 30-mile intervals.

The arrive and leave SOC of the EV at each pass-through point are presented in Fig. 12. Here, we can see that the SOC at the starting point is 100% SOC following our initial constraint. By the journey's end, the SOC dwindles to 5.16%, strategically positioned just above the lower threshold of our terminal stage constraint, such that no charging time is waste

for unused energy. A closer inspection of Fig. 12 reveals points where the arrival and departure SOCs are equal. This indicates that the EV bypassed charging at these points. Upon arrival to the stations, the SOCs are all near 10%, which is the lower band of the SOC in the stage constraints. On the other hand, the average departure SOC is about 37.7%. This observation reflects that the system is trying to capture the max charging power where the curve is at the highest, as seen in Fig. 5.

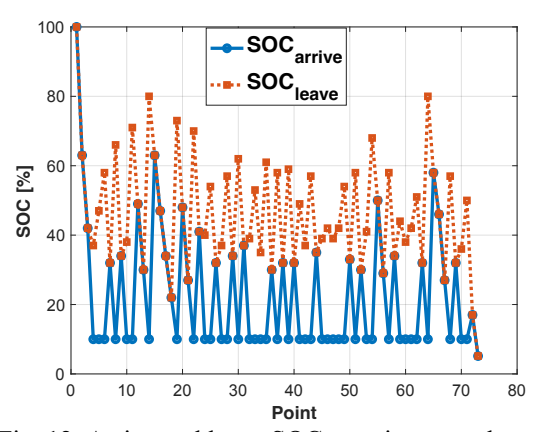


Fig. 12. Arrive and leave SOC crossing pass-through points.

While the arrival SOC at each point is almost identical, a higher leave SOC leads to a longer charging time, as shown in Fig. 13. Here, we use the term "pure charging time" to represent the charging time just used to charge the EV, and the word "charging added time" to represent the charging time involved with the detour time and extra duration demanded by charging activities. Variations in these times are influenced by the detour lengths to each chosen charging station. The shortest detour to a proximate charging station per segment is plotted in Fig. 14. Some segments, notably those associated with points 13 and 55, entail notably lengthy detours. Nevertheless, our algorithm adeptly circumvents these conditions by strategically bypassing these zones rather than unnecessarily charging the EV at these stations.

As a result, the total travel time using our proposed system is 37.61 hours, which shaves off roughly 5 hours compared to the EV record set in 2021 – an improvement of 11%. It's worth noting that the 37.61 hours of travel time we achieved, as well as the EV record set in 2021, resulted from exceptionally high driving speeds that violate traffic regulations. When we restrict the vehicle to legally permissible speed limits for every road segment of the entire trip, the fastest travel time our system can achieve is 46 hours and 11 mins—just 3 hour and 54 minutes slower than the Cannonball Run EV record.

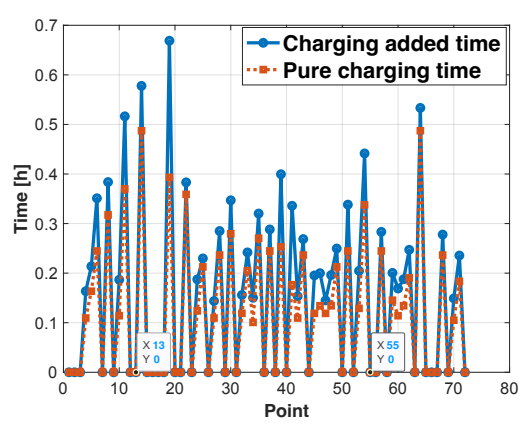


Fig. 13. Charging time crossing pass-through points.

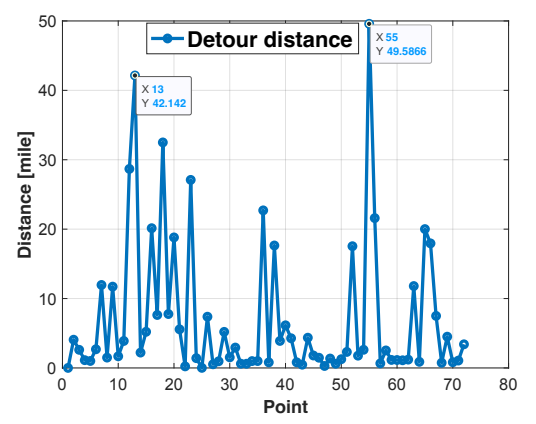


Fig. 14. Detour distance to the charging stations crossing pass-through points.

2) Impacts of the nonlinear charging power profile: This subsection is dedicated to illustrating the importance of the nonlinear charging power profile in the optimization of EV route planning and charge scheduling. For comparative purposes, we incorporate a constant charging power profile into our optimization framework. The constant power is set at 159.9 kW, representative of the average charging power observed in Fig. 5, to facilitate a meaningful benchmark comparison.

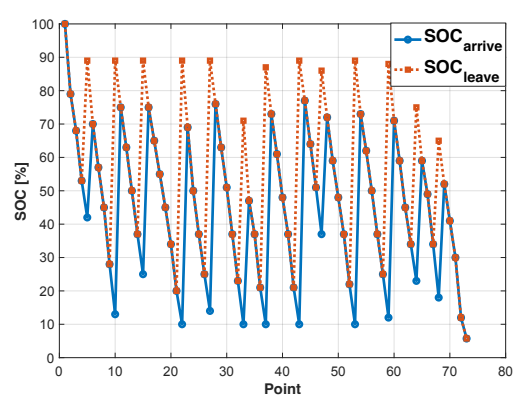


Fig. 15. Arrive and leave SOC crossing pass-through points while a constant charging power profile is used.

Fig. 15 illustrates the leave and arrive SOC patterns resulting from this optimization, which employs the constant charging power profile. One striking feature of these results is the consistent clustering of the departure SOC around the 90% mark, coinciding with the upper limit set within our stage constraints. Notably, using the constant charging power profile prescribes a total of 13 charging stops for the EV, a significant reduction compared to the 48 instances produced by the optimization result using the nonlinear charging power profile, as presented in Fig. 12. Besides, the total traveling time is 40.43 hours, which is 2.82 hours longer than the results we obtained using the nonlinear charging profile.

We can see fewer charging stops and longer total travel time under the constant power profile. The result is due to the lack of specialized SOC zones, which offer varying charging rates in a nonlinear charging profile. Under this simplified assumption, the strategy defaults to maximizing the charge at each opportunity, aiming to extend the range between stops, given the added time and energy expenditure necessitated by detours to charging stations and battery preconditioning. However, this overlooks the nuanced efficiencies of real-world charging, where charging to full capacity at every stop is neither practical nor efficient. This contrasts with the nonlinear approach, where the charging strategy is tailored to exploit faster charging rates at lower SOCs and avoid inefficiencies at higher SOCs, mirroring actual EV charging behavior and leading to a more efficient journey.

3) Impact of basic routing path partition intervals: This subsection analyzes the sensitivity of the route partition intervals on overall system performance. We assessed intervals ranging from 10 to 80 miles.

Fig. 16 reveals a clear trend: shorter partition intervals correspond to reduced overall travel times. Specifically, a 10-mile partition yields a travel time of just 36.02 hours. In stark contrast, an 80-mile interval closely mirrors the benchmark time of approximately 42.6 hours.

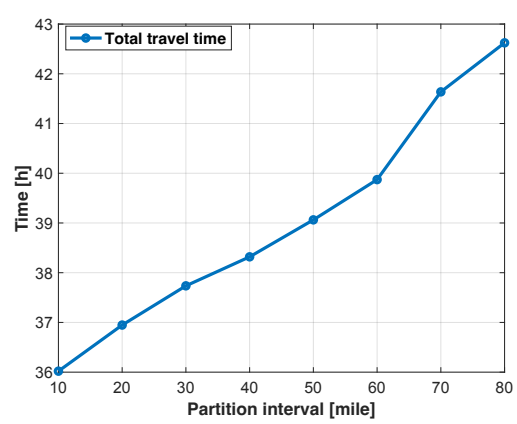


Fig. 16. Partition interval vs. Total travel time.

This phenomenon can be attributed to several key factors:

 Higher charging power in low SOC range: Shorter partition intervals permit EVs to depart charging stations with lower SOC levels without the concern of depleting the battery before the subsequent charging point. As Fig. 17 illustrates, EVs with partition intervals ranging from 10 to 30 miles predominantly remain within the SOC bracket that facilitates rapid charging.

- 2. **Higher average driving speed**: Increased charging opportunities empower the EV to maintain higher speeds, even when these speeds demand increased energy consumption. The upper subplot in Fig. 18 indicates that a smaller partition interval directly translates to a higher average trip speed. The optimization logic leans toward charging the EV if the additional charging time, induced by elevated energy usage, is less than time savings from swifter driving.
- Shorter total detour distances: The lower subplot in Fig. 18 suggests that shorter intervals yield reduced aggregate detour distances when charging is required. Shorter partition intervals provide more charging stations for selection. With the enlarged solution space, the system can deftly steer the EV clear of stations demanding extensive detours. Conversely, when choices are constricted and charging is imperative to prevent depletion, the system's flexibility compromised. It is worth noting that the Haversine calculations have higher accuracy over shorter spans and on more linear roadways. Extended intervals could inadvertently underestimate detour distances and lead to suboptimal station selections.

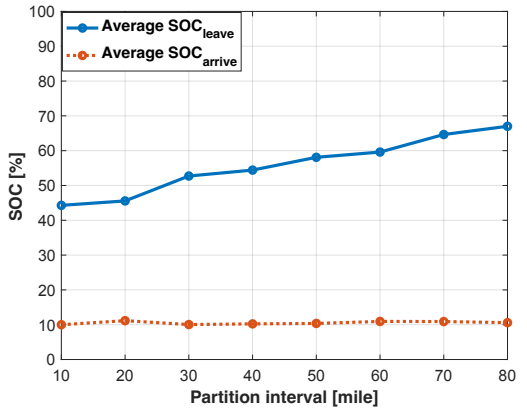


Fig. 17. Partition interval vs. Average leave and arrive SOC for charging cases.

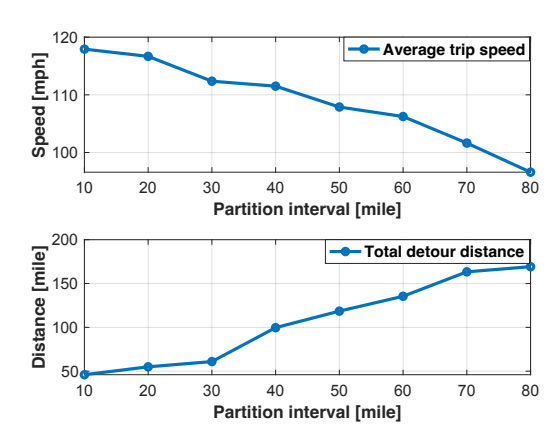


Fig. 18. Partition interval vs. Average Speed and total detour time.

However, choosing the smallest partition interval is not without some costs. As the upper subplot in Fig. 19 illustrates, the computation times increase exponentially with decreasing intervals. The surge in decision variables, especially binary ones, boosts the computational burden, especially when employing MILP for problem-solving. Further, the proliferation of pass-through points and charging stations triggers an increased need for Google Maps API queries, thereby elevating the associated monetary costs. Given the estimated cost of the Google Maps API at \$5 per 1,000 requests, the costs across varying partition intervals are depicted in the lower subplot in Fig. 19.

As a result, we selected a 30-mile partition interval for the main results to balance performance, accuracy, and cost. This decision adeptly balances travel time optimization, computational efficiency, and the costs tied to API queries. However, for racing purposes, where costs aren't a primary concern, the 10-mile partition interval may be the most favorable choice, yielding the shortest total travel time of 36.02 hours.

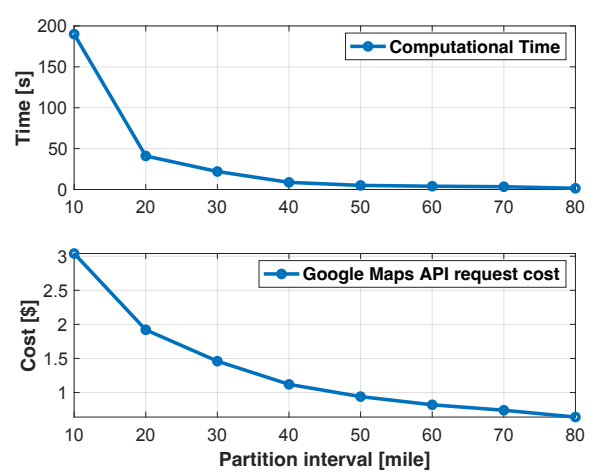


Fig. 19. Partition interval vs. Total computational time and total monetary cost of using Google Maps API.

#### IV. CONCLUSION

In this work, our primary goal is to understand the nature and develop strategies for minimizing total travel time in long-distance EV driving. We develop a comprehensive framework that synergizes real-time V2C interactions, route data processing, energy consumption modeling, and a novel charging time prediction model. Notably, our charging time model adeptly accommodates various nonlinear charging profiles. By transforming the optimization challenge into a MILP framework, our system achieves low computational cost, facilitating real-time application. This framework enabled us to tackle crucial questions effectively: How fast should we drive? When and where should we charge our EV? And to what SOC level should we charge at these points?

As a result, our proposed system not only outperformed existing real-world records for EVs set in the Cannonball Challenge by 11% but also underscored the critical impact of nonlinear charging profiles on route optimization. This comparison between strategies derived from nonlinear versus constant charging profiles demonstrates the necessity of accounting for nonlinear charging dynamics. Importantly, our framework is adaptable to a wide range of applications beyond competitive scenarios like the Cannonball Challenge. Its potential extends from personal road trips to commercial logistics, including long-haul trucking. Furthermore, the approach is particularly relevant to the evolving field of autonomous driving [50], transitioning from traditional human-centric constraints [51] to more sophisticated, vehicle-centric operational paradigms.

In future studies, by leveraging V2X and the Open Charge Point Interface (OCPI) protocol, we can incorporate a broader set of real-time data and integrate more factors, such as weather conditions and waiting times at charging stations, to enhance system performance. Besides, exploring battery degradation minimization as part of a multi-objective optimization problem presents a valuable direction. Additionally, adapting the proposed system for broader logistics fleet management also presents a promising avenue for exploration.

## V. REFERENCE:

- [1] "The Paris Agreement | UNFCCC." Accessed: Sep. 24, 2023. [Online]. Available: https://unfccc.int/process-and-meetings/the-parisagreement
- [2] K. O. Yoro and M. O. Daramola, "Chapter 1 CO2 emission sources, greenhouse gases, and the global warming effect," in *Advances in Carbon Capture*, M. R. Rahimpour, M. Farsi, and M. A. Makarem, Eds., Woodhead Publishing, 2020, pp. 3–28. doi: 10.1016/B978-0-12-819657-1.00001-3.
- [3] A. Khaligh and Z. Li, "Battery, Ultracapacitor, Fuel Cell, and Hybrid Energy Storage Systems for Electric, Hybrid Electric, Fuel Cell, and Plug-In Hybrid Electric Vehicles: State of the Art," *IEEE Transactions on Vehicular Technology*, vol. 59, no. 6,

- pp. 2806–2814, Jul. 2010, doi: 10.1109/TVT.2010.2047877.
- [4] B. Jones, R. J. R. Elliott, and V. Nguyen-Tien, "The EV revolution: The road ahead for critical raw materials demand," *Applied Energy*, vol. 280, p. 115072, Dec. 2020, doi: 10.1016/j.apenergy.2020.115072.
- [5] L. Zhang, C. Sun, G. Cai, and L. H. Koh, "Charging and discharging optimization strategy for electric vehicles considering elasticity demand response," eTransportation, vol. 18, p. 100262, Oct. 2023, doi: 10.1016/j.etran.2023.100262.
- [6] S. Zheng, X. Zhu, Z. Xiang, L. Xu, L. Zhang, and C. H. T. Lee, "Technology trends, challenges, and opportunities of reduced-rare-earth PM motor for modern electric vehicles," *Green Energy and Intelligent Transportation*, vol. 1, no. 1, p. 100012, Jun. 2022, doi: 10.1016/j.geits.2022.100012.
- [7] H. He *et al.*, "China's battery electric vehicles lead the world: achievements in technology system architecture and technological breakthroughs," *Green Energy and Intelligent Transportation*, vol. 1, no. 1, p. 100020, Jun. 2022, doi: 10.1016/j.geits.2022.100020.
- [8] J. S. Dorr Bryon, "Cannonball Run Record: A Guide to America's Ultimate Illegal Street Race," GearJunkie. Accessed: Sep. 24, 2023. [Online]. Available: https://gearjunkie.com/motors/cannonball-run-record
- [9] F. Amariei, "EV Cannonball Record Attempt With the Lucid Air Flops, Can't Blame the Car," autoevolution. Accessed: Sep. 24, 2023. [Online]. Available: https://www.autoevolution.com/news/evcannonball-record-attempt-with-the-lucid-air-flopscan-t-blame-the-car-214072.html
- [10] T. S. Bryden, G. Hilton, A. Cruden, and T. Holton, "Electric vehicle fast charging station usage and power requirements," *Energy*, vol. 152, pp. 322–332, Jun. 2018, doi: 10.1016/j.energy.2018.03.149.
- [11] "Full article: The Ripple effect in supply chains: trade-off 'efficiency-flexibility-resilience' in disruption management." Accessed: Sep. 24, 2023. [Online]. Available: https://www.tandfonline.com/doi/full/10.1080/00207 543.2013.858836
- [12] J. Liu, G. Lin, S. Huang, Y. Zhou, Y. Li, and C. Rehtanz, "Optimal EV Charging Scheduling by Considering the Limited Number of Chargers," *IEEE Transactions on Transportation Electrification*, vol. 7, no. 3, pp. 1112–1122, Sep. 2021, doi: 10.1109/TTE.2020.3033995.
- [13] T. W. House, "Fact Sheet: The Bipartisan Infrastructure Deal," The White House. Accessed: Sep. 24, 2023. [Online]. Available: https://www.whitehouse.gov/briefingroom/statements-releases/2021/11/06/fact-sheet-thebipartisan-infrastructure-deal/
- [14] "Bipartisan Infrastructure Law National Electric Vehicle Infrastructure (NEVI) Formula Program Fact

- Sheet | Federal Highway Administration." Accessed: Sep. 24, 2023. [Online]. Available: https://www.fhwa.dot.gov/bipartisan-infrastructure-law/nevi\_formula\_program.cfm
- [15] Y. Xiao, Y. Zhang, I. Kaku, R. Kang, and X. Pan, "Electric vehicle routing problem: A systematic review and a new comprehensive model with nonlinear energy recharging and consumption," *Renewable and Sustainable Energy Reviews*, vol. 151, p. 111567, Nov. 2021, doi: 10.1016/j.rser.2021.111567.
- [16] M. Schneider, A. Stenger, and D. Goeke, "The Electric Vehicle-Routing Problem with Time Windows and Recharging Stations," *Transportation Science*, vol. 48, no. 4, pp. 500–520, Nov. 2014, doi: 10.1287/trsc.2013.0490.
- [17] Y. Xiao, X. Zuo, I. Kaku, S. Zhou, and X. Pan, "Development of energy consumption optimization model for the electric vehicle routing problem with time windows," *Journal of Cleaner Production*, vol. 225, pp. 647–663, Jul. 2019, doi: 10.1016/j.jclepro.2019.03.323.
- [18] G. Hiermann, J. Puchinger, S. Ropke, and R. F. Hartl, "The Electric Fleet Size and Mix Vehicle Routing Problem with Time Windows and Recharging Stations," *European Journal of Operational Research*, vol. 252, no. 3, pp. 995–1018, Aug. 2016, doi: 10.1016/j.ejor.2016.01.038.
- [19] S. Erdoğan and E. Miller-Hooks, "A Green Vehicle Routing Problem," *Transportation Research Part E: Logistics and Transportation Review*, vol. 48, no. 1, pp. 100–114, Jan. 2012, doi: 10.1016/j.tre.2011.08.001.
- [20] "Joint Design for Electric Fleet Operator and Charging Service Provider: Understanding the Non-Cooperative Nature." Accessed: Sep. 24, 2023. [Online]. Available: https://ieeexplore.ieee.org/abstract/document/993199 6/
- [21] J. Yang and H. Sun, "Battery swap station location-routing problem with capacitated electric vehicles," *Computers & Operations Research*, vol. 55, pp. 217–232, Mar. 2015, doi: 10.1016/j.cor.2014.07.003.
- [22] H. Yee, J. Gijsbrechts, and R. Boute, "Synchromodal transportation planning using travel time information," *Computers in Industry*, vol. 125, p. 103367, Feb. 2021, doi: 10.1016/j.compind.2020.103367.
- [23] "Optimal Electric Vehicles Route Planning with Traffic Flow Prediction and Real-Time Traffic Incidents | International Journal of Electrical and Computer Engineering Research." Accessed: Sep. 24, 2023. [Online]. Available: https://ijecer.org/ijecer/article/view/93
- [24] "Electric Vehicle Route Selection and Charging Navigation Strategy Based on Crowd Sensing." Accessed: Sep. 24, 2023. [Online]. Available: https://ieeexplore.ieee.org/abstract/document/787983

- [25] J. Shi, B. Xu, Y. Shen, and J. Wu, "Energy management strategy for battery/supercapacitor hybrid electric city bus based on driving pattern recognition," *Energy*, p. 122752, Nov. 2021, doi: 10.1016/j.energy.2021.122752.
- [26] J. Shi, J. Wu, B. Xu, and Z. Song, "Cybersecurity of Hybrid Electric City Bus with V2C Connectivity," *IEEE Transactions on Intelligent Vehicles*, pp. 1–16, 2023, doi: 10.1109/TIV.2023.3281032.
- [27] B. Lin, B. Ghaddar, and J. Nathwani, "Electric vehicle routing with charging/discharging under timevariant electricity prices," *Transportation Research Part C: Emerging Technologies*, vol. 130, p. 103285, Sep. 2021, doi: 10.1016/j.trc.2021.103285.
- [28] "Mathematics | Free Full-Text | Electric-Vehicle Routing Planning Based on the Law of Electric Energy Consumption." Accessed: Sep. 24, 2023. [Online]. Available: https://www.mdpi.com/2227-7390/10/17/3099
- [29] S. Shao, W. Guan, and J. Bi, "Electric vehicle-routing problem with charging demands and energy consumption," *IET Intelligent Transport Systems*, vol. 12, no. 3, pp. 202–212, 2018, doi: 10.1049/iet-its.2017.0008.
- [30] R. Basso, B. Kulcsár, B. Egardt, P. Lindroth, and I. Sanchez-Diaz, "Energy consumption estimation integrated into the Electric Vehicle Routing Problem," *Transportation Research Part D: Transport and Environment*, vol. 69, pp. 141–167, Apr. 2019, doi: 10.1016/j.trd.2019.01.006.
- [31] M. H. Mobarak and J. Bauman, "Vehicle-Directed Smart Charging Strategies to Mitigate the Effect of Long-Range EV Charging on Distribution Transformer Aging," *IEEE Transactions on Transportation Electrification*, vol. 5, no. 4, pp. 1097–1111, Dec. 2019, doi: 10.1109/TTE.2019.2946063.
- [32] J. Shi, M. Tian, S. Han, T.-Y. Wu, and Y. Tang, "Electric vehicle battery remaining charging time estimation considering charging accuracy and charging profile prediction," *Journal of Energy Storage*, vol. 49, p. 104132, May 2022, doi: 10.1016/j.est.2022.104132.
- [33] J. Shi, T. Zeng, and S. Moura, "Electric fleet charging management considering battery degradation and nonlinear charging profile," *Energy*, vol. 283, p. 129094, Nov. 2023, doi: 10.1016/j.energy.2023.129094.
- [34] S. Schoenberg and F. Dressler, "Planning Ahead for EV: Total Travel Time Optimization for Electric Vehicles," in 2019 IEEE Intelligent Transportation Systems Conference (ITSC), Auckland, New Zealand: IEEE Press, Oct. 2019, pp. 3068–3075. doi: 10.1109/ITSC.2019.8917335.
- [35] C. Hecht, K. Victor, S. Zurmühlen, and D. U. Sauer, "Electric vehicle route planning using real-world charging infrastructure in Germany," *eTransportation*, vol. 10, p. 100143, Nov. 2021, doi: 10.1016/j.etran.2021.100143.

- [36] T. Chen, B. Zhang, H. Pourbabak, A. Kavousi-Fard, and W. Su, "Optimal Routing and Charging of an Electric Vehicle Fleet for High-Efficiency Dynamic Transit Systems," *IEEE Transactions on Smart Grid*, vol. 9, no. 4, pp. 3563–3572, Jul. 2018, doi: 10.1109/TSG.2016.2635025.
- [37] J. Lin, W. Zhou, and O. Wolfson, "Electric Vehicle Routing Problem," *Transportation Research Procedia*, vol. 12, pp. 508–521, Jan. 2016, doi: 10.1016/j.trpro.2016.02.007.
- [38] Y. He, K. M. Kockelman, and K. A. Perrine, "Optimal locations of U.S. fast charging stations for long-distance trip completion by battery electric vehicles," *Journal of Cleaner Production*, vol. 214, pp. 452–461, Mar. 2019, doi: 10.1016/j.jclepro.2018.12.188.
- [39] "Google Maps," Google Maps. Accessed: Aug. 07, 2023. [Online]. Available: https://www.google.com/maps/@37.3660498,-122.0273929,13.48z?entry=ttu
- [40] Y. Zheng, Y. Song, D. J. Hill, and K. Meng, "Online Distributed MPC-Based Optimal Scheduling for EV Charging Stations in Distribution Systems," *IEEE Transactions on Industrial Informatics*, vol. 15, no. 2, pp. 638–649, Feb. 2019, doi: 10.1109/TII.2018.2812755.
- [41] J. Xu, M. Saleh, A. Wang, R. Tu, and M. Hatzopoulou, "Embedding local driving behaviour in regional emission models to increase the robustness of on-road emission inventories," *Transportation Research Part D: Transport and Environment*, vol. 73, pp. 1–14, Aug. 2019, doi: 10.1016/j.trd.2019.05.011.
- [42] J. Shi, B. Xu, X. Zhou, and J. Hou, "A cloud-based energy management strategy for hybrid electric city bus considering real-time passenger load prediction," *Journal of Energy Storage*, vol. 45, p. 103749, Jan. 2022, doi: 10.1016/j.est.2021.103749.
- [43] B. Xu, J. Shi, S. Li, and H. Li, "A Study of Vehicle Driving Condition Recognition Using Supervised

- Learning Methods," *IEEE Transactions on Transportation Electrification*, pp. 1–1, 2021, doi: 10.1109/TTE.2021.3127194.
- [44] "Drive Cycle Analysis Tool DriveCAT."

  Accessed: Apr. 17, 2023. [Online]. Available: https://www.nrel.gov/transportation/drive-cycletool/index.html
- [45] J. Shi and Z. Teng, "Charging Profiles of a 2023 Tesla Model S Using Tesla V3 Superchargers," Dec. 2023, doi: 10.5281/zenodo.10403157.
- [46] "A Rented Tesla Model S Just Shattered the EV Cannonball Record," Road & Track. Accessed: Sep. 24, 2023. [Online]. Available: https://www.roadandtrack.com/news/a38095522/ev-cannonball-record-tesla-model-s/
- [47] T. Zhu *et al.*, "An Optimized Energy Management Strategy for Preheating Vehicle-Mounted Li-ion Batteries at Subzero Temperatures," *Energies*, vol. 10, no. 2, Art. no. 2, Feb. 2017, doi: 10.3390/en10020243.
- [48] "Model S Owner's Manual," Tesla. Accessed: Aug. 08, 2023. [Online]. Available: https://www.tesla.com/ownersmanual/models/en\_us/GUID-91E5877F-3CD2-4B3B-B2B8-B5DB4A6C0A05.html
- [49] "Electric Cars, Solar & Clean Energy," Tesla. Accessed: Aug. 07, 2023. [Online]. Available: https://www.tesla.com/
- [50] S. A. Bagloee, M. Tavana, M. Asadi, and T. Oliver, "Autonomous vehicles: challenges, opportunities, and future implications for transportation policies," *J. Mod. Transport.*, vol. 24, no. 4, pp. 284–303, Dec. 2016, doi: 10.1007/s40534-016-0117-3.
- [51] D. Wolfinger, F. Tricoire, and K. F. Doerner, "A matheuristic for a multimodal long haul routing problem," *EURO Journal on Transportation and Logistics*, vol. 8, no. 4, pp. 397–433, Dec. 2019, doi: 10.1007/s13676-018-0131-1.